A New Method of Identifying the Site of Tyrosyl Radicals in Proteins

Dimitri A. Svistunenko and Chris E. Cooper
Department of Biological Sciences, University of Essex, Colchester, Essex, United Kingdom

ABSTRACT   Protein-bound tyrosyl radicals catalyze many important enzymatic reactions. They can also initiate oxidative damage to cells. Here we report a new method of computer simulation of tyrosyl radical electron paramagnetic resonance spectra. The method enables the determination of the rotational conformation of the phenoxyl ring in a radical with unprecedented accuracy ($\sim2°$). When coupled with a new online database, all tyrosine residues in a protein can be screened for that particular conformation. For the first time we show relationships between the spin density on atom C1 (ρ_{C1}) and the principal g-factors measured by electron paramagnetic resonance spectroscopy (ρ_{C1} on g_x is shown to be linear). The new method enables the accurate determination of ρ_{C1} in all known tyrosyl radicals, evaluates the likelihood of a hydrogen bond, and determines the possibility of a ρ_{C1} distribution in the radicals. This information, together with the accurately determined rotational conformation, is frequently sufficient to allow for an unambiguous identification of the site of radical formation. The possibility of a similar relationship between ρ_C and g_x in other radicals, e.g., tryptophanyl, is discussed.

INTRODUCTION

Many proteins make use of free radicals as part of their catalytic mechanism (Frey, 2001). Reactions catalyzed include electron transfer (e.g., photosynthetic reaction center), biosynthesis (e.g. ribonucleotide reductase, i.e., RNR; prostaglandin H synthase, i.e., PGHS; and horseradish peroxidase), the generation of reactive intermediates in host defense (e.g., myeloperoxidase, lactoperoxidase), or the removal of reactive oxygen species (e.g., catalase). The uncontrolled formation of protein-bound free radicals is increasingly being seen as playing a role in the etiology of a range of diseases, e.g., rhabdomyolysis or subarachnoid hemorrhage (Reeder et al., 2002).

Tyrosine (Tyr) is undoubtedly the most frequently reported site of free radical formation in proteins. Some tyrosyl radicals are associated with the enzymatic activity. Others are formed transiently during enzyme turnover or inhibition. Tyrosyl radicals have been found in RNR from different sources (Allard et al., 1996; Reichard and Ehrenberg, 1983; Sahlin et al., 1982); in ovine and human PGHS (Dorlet et al., 2002; Hsi et al., 1994); in *Mycobacterium tuberculosis* catalase-peroxidase treated with peroxyacetic acid (Chouchane et al., 2002); in *Dactylium dendroides* galactose oxidase (Babcock et al., 1992; Whittaker et al., 1996a); in *Phanerochaete chrysosporium* glyoxal oxidase (Whittaker et al., 1996b); in bovine catalase treated with H_2O_2 (Ivancich et al., 1996); in human hemoglobin (Hb), soybean leghemoglobin (Lb), horse and sperm whale myoglobins (Mb) treated with H_2O_2 (Davies and Puppo, 1992; Gunther et al., 2000, 1998; Svistunenko et al., 2002); and in photosystem II (PSII) (Hoganson and Babcock, 1992; Tommos et al., 1995).

The method of choice for detecting free radicals in proteins is electron paramagnetic resonance (EPR) spectroscopy.

However, the assignment of an EPR spectrum to a tyrosyl radical is not always straightforward, since tyrosyl radicals in different proteins show very different EPR spectra. Furthermore, even when an EPR spectrum is definitively assigned to a tyrosyl radical, the question remains: which tyrosine is responsible for the radical? Conventionally, mutation of different tyrosine residues is used to answer this question. However, although site-directed mutagenesis can rule out residues for which the mutation has no effect on the observed EPR spectrum, perturbation of an EPR spectrum is not unequivocal evidence that the radical is in the mutation site. For example, the mutated amino acid may be involved in the primary chemistry of radical formation which is then being transferred to the final stable site. In such case the mutation will perturb the EPR spectrum even though the observed radical is far away from the mutation. This appears to be the case, for example, with sperm whale Mb treated with hydrogen peroxide where the Tyr[103] to Phe[103] mutation removes the observed tyrosyl radical, yet the radical is likely to be on Tyr[151] (Svistunenko et al., 2002).

The variability of the EPR spectra of the tyrosyl radicals in different proteins (Fig. 1) is traditionally associated with the ability of the phenolic group in tyrosine to rotate around the $C_\beta-C1$ bond (Fig. 2).

When a radical is formed on a Tyr, the oxygen proton is lost. The EPR spectrum is therefore defined by the hyperfine interaction of the unpaired electron with the four ring protons and with the β-protons of the methylene group. The hyperfine interaction with the β-protons depends on the rotation angle θ (Fig. 2), according to the McConnell relation (McConnell and Cheshunt, 1958),

$$A_{iso}^{\beta} = \rho_{C1}(B' + B''\cos^2\theta), \quad (1)$$

where A_{iso}^{β} is the isotropic hyperfine splitting constant, ρ_{C1} is the spin density on atom C1, and B' and B'' are constants,
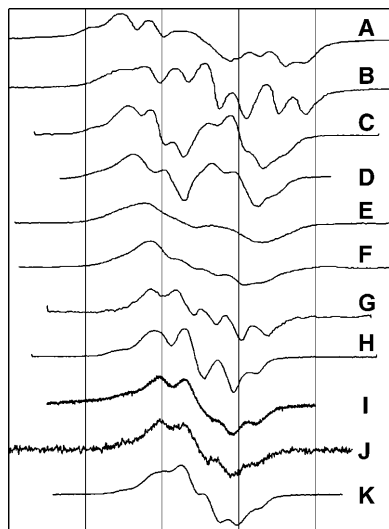
FIGURE 1 The X-band EPR spectra of Tyr radicals in different proteins. (A) *P. denitrificans* C*c*O+H_2O_2 (MacMillan et al., 1999); (B) horse metMb+H_2O_2 (Miki et al., 1989); (C) mouse TA3 cells RNR (Sahlin et al., 1987); (D) *E. coli* RNR (Hoganson and Babcock, 1992); (E) ovine PGHS, wide doublet (Kulmacz et al., 1990); (F) ovine PGHS, narrow singlet (Dorlet et al., 2002); (G) soybean metLb+H_2O_2 (Davies and Puppo, 1992); (H) *S. typhimurium* RNR (Allard et al., 1996); (I) *A. thaliana* photosystem II $Y_D^{.}$ radical (Svistunenko et al., 2002); (J) metHb+H_2O_2 (Svistunenko et al., 2002); and (K) bovine catalase+peroxyacetic acid (Ivancich et al., 1996). The spectra were plotted on a common magnetic field axis as described in Software and Methods. The gridlines are drawn at a 20-Gauss interval.

with B' being commonly neglected in practical applications and B'' being equal to 58 G (Fessenden and Schuler, 1963). The A_{iso}^{β}-values for both β-protons can be determined via a simulation of the experimental X-band (~9 GHz) EPR spectrum. The two unknowns, ρ_{C1} and θ, can then be found from a system involving the use of Eq. 1 written for the two protons. Knowing the value of θ for a tyrosyl radical is important for identification of the responsible tyrosine residue, because this angle can be directly measured for any tyrosine, if the three-dimensional structure of the protein is known.

Thus, tyrosyl radicals with different rotational conformations of the phenoxyl ring will have EPR spectra with different patterns of hyperfine structure. This rationalization
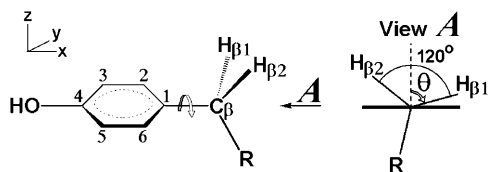

FIGURE 2 A definition of the ring rotation angle in tyrosine. The ring rotation angle θ in tyrosine is defined in this article for view A. It is the angle for proton β_1; it is positive when measured clockwise from the upward perpendicular to the ring plane when the C_β–R bond is below the horizontally oriented ring plane.

of the variability of the EPR lineshapes (Fig. 1) has been generally validated in a number of publications by computer simulation of the experimental X-band EPR spectra of tyrosyl radicals (Sahlin et al., 1982; DeGray et al., 1992; Hoganson and Babcock, 1992; Schmidt et al., 1996; Allard et al., 1996; Ivancich et al., 1996, 2001a,b; Himo et al., 1997; Shi et al., 2000; Gunther et al., 2000; Di Bilio et al., 2001; Warncke and Perry, 2001; Svistunenko et al., 2002). Unfortunately, it is usually necessary to specify ~30 parameters to simulate a tyrosyl radical EPR spectrum. Although many agree that most of these parameters are conserved, i.e., constants for all tyrosyl radicals, there are still 12 non-conserved parameters which have to be specified individually for every type of tyrosyl radical. This considerable number of degrees of freedom unavoidably results in a low accuracy in the parameters determined. The extent of these errors results in a significant degree of ambiguity over the conclusions this type of study can possibly hope to achieve.

When analyzing the simulation parameters previously reported for different tyrosyl radicals we found that no single set of the rotation-independent parameters could be successfully used to simulate all known tyrosyl radical spectra when only the β-protons' splitting constants are allowed to vary. In other words, the variability of the lineshapes of the X-band EPR spectra of tyrosyl radicals cannot be exclusively explained by different angles of rotation of the phenoxyl group.

We therefore report here a completely new approach to the simulation of the tyrosyl radical EPR spectra. We have developed an algorithm enabling us to determine all simulation parameters, using only two input variables: the unpaired spin density on atom C1 and the phenoxyl ring rotation angle. These two input variables, being clear physical and geometrical values and not mathematical constructs, can only be varied within known limited intervals. Thus, we have managed to shrink the 30-dimensional space of tyrosyl radicals existence to a tiny two-dimensional plane with clearcut borders at all four sides. The fact of the tyrosyl radical spectra dependence on ρ_{C1} and on the angle of the phenoxyl ring rotation is already well established. The importance of our results is in our new finding that every spectrum is completely defined by just these two values. All nonconserved parameters necessary for the simulation of the spectrum can be derived (calculated) from the spin density and the rotation angle. This has only become possible because we have found new empirical relationships between the parameters previously considered independent; the most important of these is the relationship between ρ_{C1} and the g-factor components.

By using the algorithm, it is possible to define whether a tyrosyl radical is responsible for the observed EPR spectrum and, if so, the most likely site harboring the radical can be identified on the protein. Additionally, the use of the algorithm allows us for the first time to predict an EPR spectrum, i.e., to simulate a lineshape that has not been experimentally determined yet.

SOFTWARE AND METHODS

Software used

UN-SCAN-IT Automated Digitizing System, Version 5.0 (Silk Scientific Corporation, http://www.silkscientific.com/) was used to digitize scanned EPR spectra published in the literature. The program *simpow6* (Mark Nilges, Illinois EPR Research Center, http://ierc.scs.uiuc.edu/~nilges/software.html) was used for the EPR spectra simulation. Swiss-PdbViewer 3.7 (http://ca.expasy.org/spdbv/text/disclaim.htm) was used to analyze the three-dimensional structure of the proteins and to measure the dihedral angles that were used to calculate θ.

All spreadsheet-calculators (see Supplementary Material for these tools) were created in Microsoft Excel 2000:

- *theta_in_tyr.xls*—file-calculator for finding θ and ρ_{C1} for any pair of values $A_{iso}^{\beta1}$ and $A_{iso}^{\beta2}$ (four solutions) or to calculate $A_{iso}^{\beta1}$ and $A_{iso}^{\beta2}$ for fixed θ- and ρ_{C1}-values (single solution).
- *g_and_k.xls*—file-calculator for finding g_x, g_y, and g_y from K, or to calculate g_y, g_y, and K from g_x.
- *algorithm.xls*—calculates all parameters necessary for a simulation of a tyrosyl radical EPR spectrum while using two input parameters, ρ_{C1} (the spin density on atom C1; range of values 0.320–0.440) and the phenoxyl ring rotation angle θ (range of values $-90°$ to $+90°$).
- *al_XB.xls* and *al_HF.xls* (at least one pair of these files per each radical)—for calculating the simulation parameters for concrete X-band and high field (HF) EPR spectra of a Tyr radical; these are the abbreviated (low graphics) versions of the *algorithm.xls* file with the values of ρ_{C1} and θ already typed in for every radical spectrum, so that the full set of the simulation parameters is readily available for every spectrum presented in the article.

Plotting Fig. 1

The X-band EPR spectra of tyrosyl radicals in different proteins, published by different authors, were scanned and digitized using UN-SCAN-IT. The magnetic field axis, common for all spectra, is not shown since the absolute value of the resonance field is different for each spectrum due to different microwave frequencies used. All spectra are aligned horizontally by an arbitrary chosen g-factor (2.005), the exact position of which on each spectrum was determined after the simulations of these spectra were performed.

Determination of the ring rotation angle θ from the dihedral angles

Protons are not resolved in the x-ray crystallographic data, so angle θ can only be determined indirectly from the dihedral angle formed by the ring plane and the R$-$C$_\beta$$-$C1 plane (Fig. 3).
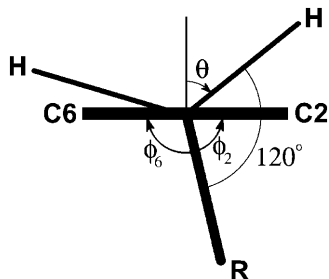

FIGURE 3 The ring rotation angle θ can be found from directly measurable dihedral angles ϕ_2 defined by R–C$_\beta$–C1–C2 and ϕ_6 defined by R–C$_\beta$–C1–C6 (note that ϕ_2 and ϕ_6 have opposite signs).

From the figure, $\theta° = 90° - (120° - \phi_2) = \phi_2 - 30°$. Since ϕ_2 is only approximately equal to $(180-\phi_6)$, because the ring atoms never form an ideal plane, we used an average value instead of ϕ_2. Thus,

$$\theta° = \frac{(180° - \phi_6) + \phi_2}{2} - 30°.$$

The angles ϕ_2 and ϕ_6 are dihedral angles and can be measured by the appropriate Swiss-PbdViewer tool. For more details see the home page of our Rotation Angle database (http://privatewww.essex.ac.uk/~svist/lev1/tyrdb/home.shtml). This database is a collection of data on the value of angle θ in tyrosine residues in various proteins.

Plotting the spectra in Table 1

All experimental and simulated X-band spectra are presented in a 80-G wide field window centered at the g-factor value of 2.00500 (the absolute values of the field being different for different spectra, and not shown). All the HF spectra are also plotted on a regular magnetic field scale, although not only the absolute values of the field but the field ranges as well are different for different spectra. The standard for the HF spectra presentation is chosen therefore as follows: the left edge of the field window for every HF spectrum corresponds to the g-factor of 2.01100, and the right edge corresponds to the g-factor of 1.99900. Consequently the middle of the window corresponds approximately, although with a good accuracy, to the g-factor of 2.005. Thus, the HF and the X-band windows are set with the center corresponding to the same g-factor, 2.005.

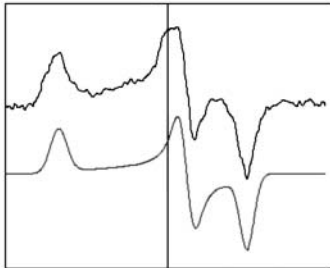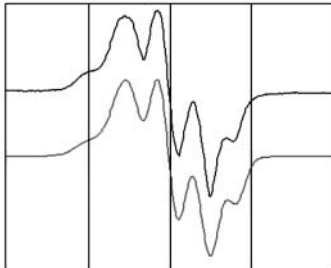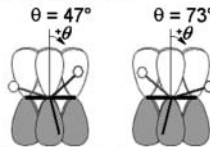### Determination of the errors in ρ_{C1} and θ (Table 1 and Fig. 7)

The errors in determination of the optimal values of ρ_{C1} and θ (Table 1) were found during the simulation of the spectra, when either ρ_{C1} or θ was varied around its optimal value, whereas the other parameter (θ or ρ_{C1}, respectively) was kept at its optimal value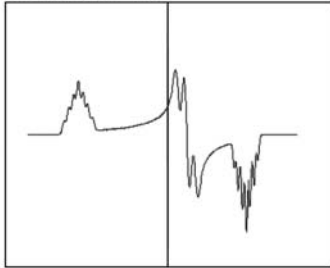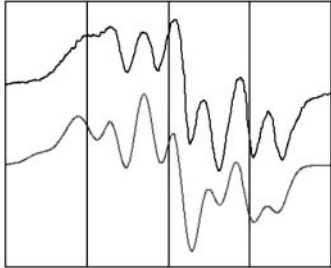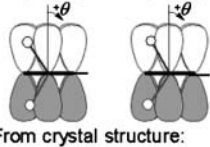. The error in ρ_{C1} was determined when the deviation in this parameter resulted in a HF spectrum noticeably different from the experimental HF spectrum. Similarly, the error in θ was determined when this parameter was varied around its optimal value and the changes in the simulated X-band spectrum were monitored. For the tyrosyl radicals with unknown HF spectra (in leghemoglobin, hemoglobin, myoglobin, and cytochrome c oxidase), the error in ρ_{C1} was found while varying this value and monitoring the changes in the X-band simulated spectrum. Since the X-band spectra are less sensitive to the g-factor changes than the HF spectra, the errors in ρ_{C1} determined for these four cases are significantly greater than when determined by monitoring the HF simulated spectrum.

RESULTS

How can we develop an algorithm that can be used to calculate all the parameters necessary for simulation of an EPR spectrum of a tyrosyl radical? To simulate a tyrosyl radical EPR spectrum, one needs to specify ~30 parameters (this number could slightly vary depending on the simulation software used). Most of these parameters are conserved; they are thought to be the same for all different tyrosyl radicals. However, different articles quote slightly different values for these conserved parameters (see Supplementary Material, *Algorithm description.pdf*, Table S1). This brings up a problem: the conserved parameters, used to simulate a tyrosyl

TABLE 1 The simulation of the HF and X-band EPR spectra of tyrosyl radical in different proteins

1. *Salmonella typhimurium* Ribonucleotide Reductase

244.997 GHz spectrum, A_m = 15 G
(Allard et al., 1996)

9.454 GHz spectrum, A_m = 2.6 G
(Allard et al., 1996)

From simulation:
$\theta = 47°$ $\theta = 73°$

From crystal structure:
ATyr105 in 1R2F; $\theta = 41.5°$

The algorithm input parameters: $\rho_{C1} = 0.350 \pm 0.002$ $\theta = 47°$(or 73°) $\pm 4°$

2. *Paracoccus Denitrificans* Cytochrome *c* Oxidase + H_2O_2

The experimental HF spectrum is not known; the simulation is for 285 GHz; A_m = 3 G

X-band spectrum, A_m = 2 G
(MacMillan et al., 1999)

From simulation:
$\theta = -38°$ $\theta = -22°$

From crystal structure:
ATyr167 in 1QLE; $\theta = -39.5°$

The algorithm input parameters: $\rho_{C1} = 0.355 \pm 0.009$ $\theta = -38°$(or -22°) $\pm 2°$

3. *Escherichia coli* Ribonucleotide Reductase

285 GHz spectrum
(Dorlet et al., 2002)

X-band spectrum
(Hoganson & Babcock, 1992)

From simulation:
$\theta = -69°$ $\theta = 9°$

From crystal structure:
ATyr122 in 1RIB; $\theta = 7.7°$

The algorithm input parameters: $\rho_{C1} = 0.358 \pm 0.002$ $\theta = -69°$(or 9°) $\pm 2°$

4. Horse heart metMb + H_2O_2

The experimental HF spectrum is not known; the simulation is for 285 GHz; A_m = 3 G

9.510 GHz spectrum, A_m = 2 G
(Miki et al., 1989)

From simulation:
$\theta = -32°$ $\theta = -28°$

From crystal structure:
Tyr103 in 1WLA; $\theta = -31.7°$

The algorithm input parameters: $\rho_{C1} = 0.370 \pm 0.010$ $\theta = -32°$(or -28°) $\pm 2°$

(*Continued*)

TABLE 1 (*Continued*)

5. Human metHb + H_2O_2

The experimental HF spectrum is not known; the simulation is for 285 GHz; A_m = 3 G	9.797465 GHz spectrum, A_m = 2 G (Svistunenko et al., 2002)	From simulation:

From simulation:
$\theta = 53°$ $\theta = 67°$

From crystal structure:
CTyr42 in 1HGB; $\theta = 49.8°$

The algorithm input parameters: ρ_{C1} = 0.375 ± 0.010 $\theta = 53°$ (or 67°) ± 2°

6. Ovine prostaglandin H synthase, "narrow singlet" (indomethacin-inhibited)

285 GHz spectrum, A_m = 20 G (Dorlet et al., 2002)	9 GHz spectrum, A_m = 3 G (Dorlet et al., 2002)	From simulation:

From simulation:
$\theta = 39°$ $\theta = 81°$

From crystal structure:
ATyr495 in 1PGF; $\theta = 38.0°$

--- ΔH_x x 2.2
The algorithm input parameters: ρ_{C1} = 0.380 ± 0.003 $\theta = 39°$ (or 81°) ± 2°

7. Mouse TA3 tumour cells, overproducing M2 subunit of mammalian RNR

244.997 GHz spectrum, A_m = 3 G (Schmidt et al., 1996)	9.5 GHz spectrum (Sahlin et al., 1987)	From simulation:

From simulation:
$\theta = -63°$ $\theta = 3°$

From crystal structure:
ATyr177 in 1XSM; $\theta = 18.3°$

The algorithm input parameters: ρ_{C1} = 0.388 ± 0.002 $\theta = -63°$ (or 3°) ± 2°

8. Photosystem II $Y_D^{\bullet}$ radical

285.363 GHz spectrum, A_m = 3.3 G; *S. oleracea* (Dorlet et al., 2000)	9.472911 GHz spectrum, A_m = 1 G *A. thaliana* (Svistunenko et al., 2002)	From simulation:

From simulation:
average   average
$\theta = 48°$ $\theta = 72°$

The crystal structure is not known

The algorithm input parameters: ρ_{C1} = 0.395 ± 0.002 (both spectra);
$\theta = 47°$ (or 73°) ± 3° for *S. oleracea* (HF spectrum) and
$\theta = 49°$ (or 71°) ± 3° for *A. thaliana* (X-band spectrum);
Angle between β-protons 117° in both cases[#]

(*Continued*)

TABLE 1 (*Continued*)

9. Bovine liver catalase + peroxyacetic acid

284.35 GHz spectrum, A_m = 10 G;
pH 5.2; (Ivancich et al., 1999)

9.222 GHz spectrum, A_m = 1.6 G
(Ivancich et al., 1996)

From simulation:
$\theta = 58°$ $\theta = 62°$

From crystal structure:
CTyr369 in 4BLC; $\theta = 58.4°$

- - - ΔH_x x 4
The algorithm input parameters: ρ_{C1} = 0.411 ± 0.004 θ = 58°(or 62°) ± 3°

10. Ovine prostaglandin H synthase, "wide doublet" (active cycloogenase)

285 GHz spectrum, A_m = 20 G
(Dorlet et al., 2002)

9.29 GHz spectrum, A_m = 2 G
(Kulmacz et al., 1990)

From simulation:
$\theta = 37°$ $\theta = 83°$

From crystal structure:
ATyr385 in 1EQG; $\theta = 26.9°$

- - - ΔH_x x 2.7
The algorithm input parameters: ρ_{C1} = 0.416 ± 0.003 θ = 37°(or 83°) ± 3°

11. Soybean metLb + H_2O_2

The experimental HF spectrum
is not known; the simulation is for
285 GHz; A_m = 3 G

X-band spectrum
(Davies & Puppo, 1992)

From simulation:
$\theta = 45°$ $\theta = 75°$

From crystal structure:
BTyr133 in 1BIN; $\theta = 51.4°$

The algorithm input parameters: ρ_{C1} = 0.420 ± 0.015 θ = 45°(or 75°) ± 3°

In each box, the simulated spectrum is shown below the experimental one. All experimental spectra are taken from the literature. When experimental spectrum is not available, only the simulated one is present. In three cases (6, 9, and 10), the dashed trace corresponds to the spectrum simulated for a greater than the algorithm predicts *x*-component of the linewidth, all other parameters being generated by the algorithm. The optimal values of the algorithm input parameters ρ_{C1} and θ, used to calculate the simulation parameters (see Supplementary Material, *Simulation Data*), are indicated under the spectra. The radicals in the table are arranged by ascending ρ_{C1}. For each radical, the two optimal θ-angles, equivalent in terms of providing the simulation parameters, are compared with the θ-angle found from the crystal structure, the latter shown under the corresponding optimal angle. The tyrosine number and the Protein Data Bank (http://www.rcsb.org/pdb/) file, e.g., 1R2F for *S. typhimurium* RNR (Eriksson et al., 1998), are indicated. Other structure files quoted in the table were first presented in the articles: 1QLE (Harrenga and Michel, 1999), 1RIB (Nordlund and Eklund, 1993), 1WLA (Maurus et al., 1997), 1HGB (Liddington et al., 1992), 1PGF (Loll et al., 1996), 1XSM (Kauppi et al., 1996), 4BLC (Ko et al., 1999), 1EQG (Selinsky et al., 2001), and 1BIN (Hargrove et al., 1997). The details of 1), how the errors in optimal ρ_{C1} and θ were determined; 2), how the spectra were plotted on a common magnetic field axis; and 3), how the θ-values were found from the crystal structure, are all described in Software and Methods.
[#]The algorithm (available in Supplementary Material as the file calculator *algorithm.xls*) allows us to vary the angle between the projections of the bonds C_β–$H_{\beta1}$ and C_β–$H_{\beta2}$ to the *y–z* plane (default value is 120°). The photosynthetic $Y_D^\cdot$ radical is the only occasion when we exercised this option.

radical spectrum, often do not work as well when used unchanged (as conserved) in a simulation of another tyrosyl radical spectrum; the simulation results in a spectrum noticeably different from the experimental one. To solve this problem, our algorithm provides for the first time values of the conserved simulation parameters that work equally well for all simulations. These values (see Supplementary Material, *Algorithm description.pdf*, Eqs. S1 and S2) are the same in all our simulations of tyrosyl radical spectra measured at all frequencies (see below).

The nonconserved parameters are those that might be different for different tyrosyl radicals. There are 12 of those—three spatial components of four physical values: hyperfine splitting constants for the two β-protons $A_j^{\beta 1}$ and $A_j^{\beta 2}$, g-factor g_j, and individual linewidth ΔH_j ($j = x, y, z$). It is generally accepted that the hyperfine splitting constant tensors for the β-protons are axial: $A_x^{\beta 1} = A_y^{\beta 1}$, $A_x^{\beta 2} = A_y^{\beta 2}$. This decreases the total number of nonconserved parameters from 12 to 10. Thus, different lineshapes of tyrosyl radicals in different protein system are caused by the differences in the 10 (of the 30 total) simulation parameters. To simulate a tyrosyl radical EPR spectrum means to find a point in a 10-dimensional search space.

It is reasonable to suggest that not all of these 10 nonconserved parameters are independent and that, in fact, some can be expressed as functions of the others. If we knew what these truly independent parameters were, and how the other parameters could be derived from the independent ones, this would then decrease the dimension of the search space and would significantly facilitate the simulation process. The accuracy of such a simulation would also be significantly higher, since the random error would be resulted from adding up the random errors of fewer variables.

The details of the theory behind the algorithm are given in Supplementary Material, *Algorithm description.pdf*. Below, we are giving a briefly summary of the algorithm. First, we have introduced a variable K,

$$K = (1/g_y - 1/g_x)/(1/g_z - 1/g_y). \qquad (2)$$

The usefulness of K is that it can be measured with a high accuracy directly from a high field (HF) EPR spectrum, without actually knowing the values of the g-factors, since the definition in Eq. 2 is equivalent to the ratio of the distances between components x and y and between components y and z: $(H_y–H_x)/(H_z–H_y)$.

We have measured K directly from all available HF spectra and showed that, for different radicals, the three g-factors can be represented as smooth continuous empirical functions of K. Thus we have added one new variable (K) to our set of 10 parameters, but have formulated three more equations. This brings down the number of independent variables from ten to eight.

In a similar way we demonstrate that the individual linewidth components ΔH_j ($j = x, y, z$) can be represented,

like the g-factors, as functions of K (the graphical representations of these dependences are given in Supplementary Material, *Algorithm description.pdf*):

$$\Delta H_x^b = -18.49\,K^4 + 129.51\,K^3 - 331.31\,K^2 + 362.86\,K \\ - 138.47,$$

$$\Delta H_y^b = -6.60\,K^4 + 48.00\,K^3 - 125.07\,K^2 + 135.15\,K \\ - 47.64,$$

$$\Delta H_z^b = -3.45\,K^4 + 27.61\,K^3 - 77.59\,K^2 + 88.82\,K \\ - 32.27,$$

where subscript b indicates that these are the basic linewidth components, independent of the spectrometer settings (the value of the modulation amplitude should be added to these values). Addition of these three equations to the system results in a further reduction of the number of independent variables by three; there are five variables now: K, $A_\perp^{\beta 1}$, $A_\parallel^{\beta 1}$, $A_\perp^{\beta 2}$, and $A_\parallel^{\beta 2}$.

Using highly precise data for the axial hyperfine splitting constants for the β-protons in the photosynthetic radical in three different organisms (Rigby et al., 1994), we have formulated an empirical dependence of the $A_\parallel^{\beta j}/A_\perp^{\beta j}$ ratio on the rotation angle θ (the graphical representation of this dependences is given in Supplementary Material, *Algorithm description.pdf*):

$$A_\parallel^{\beta j}/A_\perp^{\beta j} = a + b\,e^{c\theta},$$

where $a = 1.12$, $b = 9.37\ 10^{-6}$, and $c = 0.162$ degree^{-1}.

Writing this dependence for the two β-protons enables us to add two more independent equations to our system of dependences, although only adding one new independent variable θ. Therefore, we effectively have, at this step, four independent variables.

Finally, the McConnell relation written for the two protons would add two more independent equations and three new variables: $A_{iso}^{\beta 1}$, $A_{iso}^{\beta 2}$, and ρ_{C1} (angle $\theta_{\beta 2}$ for the second β-proton is not a new independent variable since it is considered to be equal to $\theta_{\beta 1} + 120°$ where $\theta_{\beta 1}$ is a variable already employed; $\theta_{\beta 1}$ equals to θ from the previous paragraph). Effectively, the number of independent variables is increased by one (there are now five variables). However, the isotropic hyperfine splitting constants are not really independent variables; they can be explicitly expressed over the parallel and perpendicular components:

$$\left.\begin{array}{l} A_{iso}^{\beta 1} = (2A_\perp^{\beta 1} + A_\parallel^{\beta 1})/3 \\ A_{iso}^{\beta 2} = (2A_\perp^{\beta 2} + A_\parallel^{\beta 2})/3 \end{array}\right\}. \qquad (3)$$

Thus we have just added two more equations without adding any new variables, which decreases the number of independent variables by two, down to the final number of three.

Now, it is completely our choice which of the variables we are going to set as independent. For convenience we select K, $A_{\text{iso}}^{\beta1}$, and $A_{\text{iso}}^{\beta2}$. We can now calculate all 10 nonconserved simulation parameters from these three input variables.

The initial version of our algorithm described above decreases the dimension of the search space in finding the right simulation parameters from 10 to 3. We have successfully used this version to simulate all previously published tyrosyl radical EPR spectra. However, one unexpected, and exciting, result led to a significant improvement in the algorithm. The dependence between ρ_{C1} and g_x turned out to be practically linear (see Supplementary Material, *Algorithm description.pdf*, Fig. S10). Therefore it follows that, instead of K, the values of g_x, g_y, and g_z can now be expressed over ρ_{C1} (Fig. 4). This is the first time that a relationship between the g-factor and the spin density has been reported. As ρ_{C1} increases, the three g-factors become closer to each other approximating the g-factor of a free electron. This behavior of the g-factor anisotropic components is similar to that we have previously described in the ferric heme proteins, when the three components tend to a single isotropic g-value of a free radical as the unpaired spin density shifts from the heme to the ligand (Svistunenko et al., 2000).

We have incorporated the first of the dependences (Eq. 4) into the latest version of our algorithm

$$g_x = -0.0359\rho_{C1} + 2.02160. \qquad (4)$$

Adding this linear dependence between ρ_{C1} and g_x to the system of dependences brings the number of truly in-

dependent variables down to two. As before, it is our choice which two parameters we consider independent. The version of the algorithm presented in this article uses the spin density ρ_{C1} and the ring rotation angle θ.

Thus, our revised algorithm is capable of calculating all 10 nonconserved parameters using only two input variables: ρ_{C1} and θ. The algorithm, as a calculating tool, is available in the form of an Excel file-calculator *algorithm.xls* (see Supplementary Material).

Fig. 5 illustrates how all the nonconserved simulation parameters, $A_j^{\beta1}$, $A_j^{\beta2}$, g_j, and ΔH_j ($j = x$, y, z), can now be derived from just two input parameters, ρ_{C1} and θ. Consequently, the best simulation can be found far more readily, as the whole search space is diminished from ten to two dimensions. Importantly, the two input parameters, as they have a very clear physical meaning, can only be varied within certain limits: the phenoxyl group rotation angle θ makes the full cycle every half of the 2π revolution and is therefore defined on the interval of $(-90°; +90°)$, whereas ρ_{C1} in all so-far known tyrosyl radicals varies within a narrow interval of 0.350–0.420, according to our results (shown below).

We have used our algorithm to simulate the lineshapes of all tyrosyl radical spectra we have been able to find in the literature, measured by both X-band and HF EPR spectroscopy (Table 1). For every radical, the same pair of optimal ρ_{C1}- and θ-values was used to generate the simulation

$g_x = -0.0359 \, \rho_{C1} + 2.02160$
$g_y = 2.9595 \, \rho_{C1}^4 - 5.03779 \, \rho_{C1}^3 + 3.10862 \, \rho_{C1}^2 - 0.83210 \, \rho_{C1} + 2.08636$
$g_z = -0.3401 \, \rho_{C1}^4 + 0.63432 \, \rho_{C1}^3 - 0.44105 \, \rho_{C1}^2 + 0.13632 \, \rho_{C1} + 1.98635$

FIGURE 4 The ρ-g chart for tyrosyl radicals in proteins. The chart shows the empirical dependences derived in the Supplementary Material, *Algorithm description.pdf*, of the g-factor components on the spin density on the C1 atom. The g-factor axis is given in a reverse order, increasing from the right to the left. The g-factor of a free electron (2.002319) is shown as a dotted vertical line.

FIGURE 5 The schematic representation of the algorithm for finding the simulation parameters for a tyrosyl radical EPR spectrum (see Supplementary Material, *Algorithm description.pdf*). The simulation parameters shown in the four boxes on the right are calculated according to the indicated formulas given in *Algorithm description.pdf*. The values of the input parameters θ and ρ_{C1} define the isotropic hyperfine splitting constant for the methylene β-protons. The x-, y-, and z-components of these constants are found from the isotropic value and from the value of θ. The ρ_{C1}-value alone defines the three components of the g-factor. The linewidth components ΔH_j are found from the basic linewidth values ΔH_j^b and from the value of the modulation amplitude A_m used; a small constant c_{Am} that accounts for inaccuracy in the modulation field calibration might be added to A_m. The basic linewidth components ΔH_j^b (intrinsic radical properties independent of the spectrometer used) are direct functions of the parameter K which is, in turn, a direct function of the three g-factors. All calculations can be preformed using the file calculator *algorithm.xls*, available as Supplementary Material online.

parameters for both HF and X-band spectra. Our method of simulation is thus a way to accurately find these two physical characteristics. Once there is a deviation from the optimal value in an input parameter, say ρ_{C1}, the algorithm would generate a different set of 10 nonconserved output (simulation) parameters; the resulting simulated spectrum based on such values will be different (worse) than the optimal simulated spectrum.

For a particular value of ρ_{C1} there are two possible values of θ in the range of $(-90°; +90°)$ that result in generation of identical sets of simulation parameters (see Supplementary Material, *theta_in_tyr.xls*, for details). EPR spectroscopy alone is unable to tell which of the two angles corresponds to the actual conformation of the radical. Therefore, if we want to find out which Tyr residue is responsible for the radical in a particular protein, we will have to compare the rotational conformations of all Tyr residues with each of two possible θ-angles. We have created an online database (http://privatewww.essex.ac.uk/~svist/lev1/tyrdb/home.shtml) that can help in performing this task. It is possible by using the database to display the list of Tyr residues in a protein, to set a target value θ_{target}, and to sort all residues by the difference $|\theta-\theta_{target}|$. The top of the sorted table of records shows the residues with the closest rotational conformation to the radical's rotational conformation as determined by our algorithm.

By having only two degrees of freedom in the simulation of the EPR spectrum, we find ourselves in a position to be able to predict an EPR spectrum that has not actually been measured before. There are four instances in Table 1 when the HF experimental spectrum is not known. The optimal ρ_{C1}- and θ-values were found from the X-band simulations and simply used to simulate (and thus predict) the HF spectra (Table 1).

For the catalase radical and for both PGHS radicals, the optimal simulation of the HF spectrum was only attained when the width of the *x*-component was markedly increased as compared with the algorithm-generated parameter (note the dashed traces for the HF spectra for the three radicals, Table 1). This is associated with a g_x-distribution in the radicals (variable population of radicals with differing values of g_x), caused by a distribution of the H-bond strength (Ivancich et al., 1999). Since we show that g_x and ρ_{C1} are related (Eq. 4), it follows that ρ_{C1} is also distributed in these particular radicals.

DISCUSSION

We have developed a semiempirical algorithm that enables us to determine accurately ρ_{C1} for all known tyrosyl radicals, evaluates the likelihood of a hydrogen bond, and determines the possibility of a ρ_{C1} distribution in the radicals. We call our algorithm semiempirical because it does more than simply interpolate existing literature data. For example, if someone wanted to establish a pure empirical relationship between ρ_{C1} and the *g*-factors they might attempt to plot the available values of these parameters (see Supplementary Material, *Algorithm description.pdf,* for Tables S3 and S5) on one plane. The result would be as shown in Fig. 6. Obviously, it is not possible to average these rough data and to construct continuous and smooth empirical dependences between ρ_{C1} and the *g*-factors. Not surprisingly, no relationship has been previously reported between these parameters.

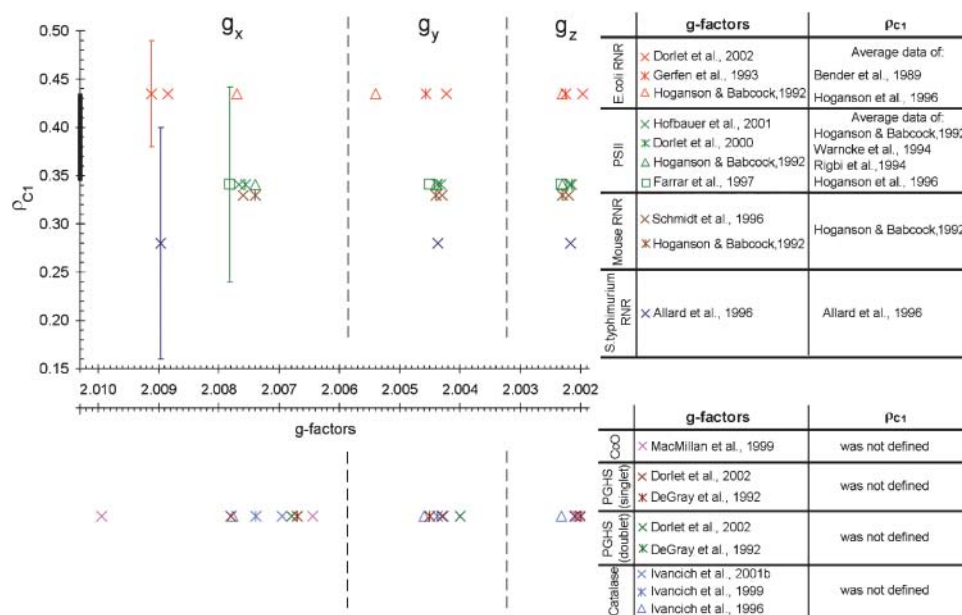FIGURE 6 The literature data on the three *g*-factors and the spin density on the C1 atom in different tyrosyl radicals. The thick segment of the ρ_{C1} axis indicates the size of Fig. 7 if plotted on this scale. The dotted vertical lines approximately indicate the g_x, g_y, and g_z areas. The data quoted can be found tabulated in Supplementary Material, *Algorithm description.pdf*, Tables S3 and S5.

When a lack of accuracy in the literature data does not allow us to find continuous and smooth relationships between parameters, we must hypothesize about what these relationships actually are. While observing the condition that our hypothetical relationships should lie within available experimental errors, we justify our hypothesis by successful simulation of all known lineshapes of tyrosyl radical EPR spectra. The same graph as shown in Fig. 6, but plotted according to our algorithm is demonstrated in Fig. 7. This figure shows that the g-factors we calculate are in good correspondence with those previously reported. At the same time, the values of ρ_{C1} we find for different tyrosyl radicals turn out to be within the range of 0.350–0.420 ($\Delta\rho_{C1} = 0.07$), which is a fivefold narrower interval than that known from the literature (0.14–0.49, $\Delta\rho_{C1} = 0.35$; see Fig. 6; see also Supplementary Material, *Algorithm description.pdf*, Table S5). More than that, we are able to specify ρ_{C1} for every radical within an error of 0.005. A high accuracy in ρ_{C1} is important, because it ensures a correspondingly high accuracy in finding the rotation angle, which, in turn, allows identification of the Tyr residue in the protein—the ultimate goal of such studies, successfully achieved in our work.

The scientific novelty of our results is in the fact that we make a leap from Fig. 6 to Fig. 7. Not only does our method find all parameters necessary for the simulation of tyrosyl radical EPR spectra, it also establishes a new empirical relationship between the spin density on atom C1 and the g-factors (Fig. 4); we look forward to an independent quantum mechanical justification of these relationships.

The value of g_x can be used to assess the electrostatic environment of tyrosyl radicals. In particular, if g_x is shifted to lower values it indicates the possibility of a hydrogen bond (Ivancich et al., 1999). Since we have established the linear dependence between ρ_{C1} and g_x (Eq. 4) the possibility of a hydrogen bond is now associated with the spin density

on C1. Fig. 7 shows that the radicals in a hydrophobic environment, such as in *S. typhimurium* and *E. coli* RNR and in C*c*O, are in the bottom of the ρ-g chart (low values of ρ_{C1}), whereas the radicals known to have a hydrogen bond due to the proximity of a protonated oxygen atom to the phenoxyl oxygen (both PGHS radicals, the $Y_D^{\cdot}$ radical in PSII, and the radicals in bovine catalase and mouse RNR) are all in the middle and the top of the chart. We suggest that all radicals with $\rho_{C1} > 0.38$ are H-bonded, and that the higher the ρ_{C1}-value, the stronger the bonding.

When the experimental HF spectrum shows the width of the g_x component is significantly broader than the algorithm predicts (catalase radical and both PGHS radicals, Table 1), this points to a distribution of g_x (and, consequently, ρ_{C1}) in the population of the radicals. Such distribution is associated with the distribution of the strength of the H-bond (Ivancich et al., 1999). Interestingly, the fact of H-bond strength distribution does not seem to be associated with the strength itself: g_x is clearly not distributed in the mouse RNR radical and in PSII-$Y_D^{\cdot}$, yet the ρ_{C1}-values for these radicals (and the strength of the H-bond) are between those for the PGHS narrow singlet and the catalase radical, both having distributed g_x-values.

For decades, researchers have been using the McConnell empirical relation for finding rotational conformation of tyrosyl radicals and ρ_{C1} from the isotropic hyperfine splitting constants for the β-protons. Such an approach is much less accurate than the one we suggest. Traditionally, a researcher has to make the following few steps to find ρ_{C1} and θ: 1), to make a hypothesis about four axial values of the hyperfine splitting constants A (two values for each of the two protons); 2), to show that the simulation is satisfactory; 3), to average the anisotropic A-values; and 4), to use those averaged, isotropic values in the McConnell equations written for two protons. Such a system of two equations then has to be
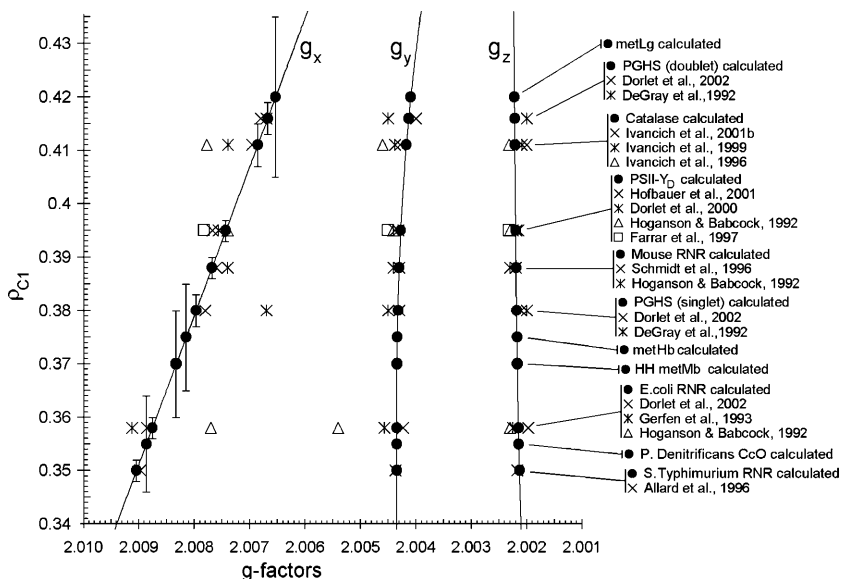
FIGURE 7 The ρ-g chart for the 11 tyrosyl radicals studied (●). The value of the spin density on atom C1 (ρ_{C1}) for each tyrosyl radical was found as the optimal input parameter of the algorithm for the EPR spectrum simulation (Table 1); the principal values of the g-factor were generated by the algorithm. The errors in ρ_{C1} are indicated at the g_x components (note significantly higher error for the radicals with unknown HF spectrum). The continuous lines are generated by the algorithm. The literature data on the principal g-factors of the Tyr radicals are also shown with the ρ_{C1}-value for each radical formally assumed the same as the value found in this work (compare with Fig. 6).

solved, and the two unknowns, the rotation angle and the spin density, can be found. The low accuracy of ρ_{C1} found by this approach is explicitly illustrated in Fig. 6. Besides, this approach results in two solutions for ρ_{C1}, one of which has to be selected and the other discarded, so additional arguments have to be considered to make this choice (see Supplementary Material, *Algorithm description.pdf*, and the file calculator *theta_in_tyr.xls* for details). In our method we solve an inverse problem: we suggest a way of finding the anisotropic hyperfine splitting components from the rotation angle. We have formulated this empirical approach on the basis of highly accurate data obtained on the photosynthetic radical found in different rotational conformations in three different organisms (Rigby et al., 1994) (see Table S2, Fig. S3, and Eq. S9 in *Algorithm description.pdf*). This has allowed us to make a hypothesis about a single value (instead of four), the rotation angle, and to find the four values of the hyperfine splitting constants for two protons.

A relationship between ρ_{C1} and the three g-factors, similar to that we have described in Eq. 4, may exist for other protein radicals. For example, the tryptophanyl radical (the second most common protein radical) also has two β-methylene protons for which the hyperfine splitting constants would depend on the rotation angle of the indole ring in the same way (according to the McConnell relation) as the constants depend on the phenoxyl ring rotation in tyrosyl radicals. We can speculate that the g_x-value of a tryptophanyl radical is related to the spin density on atom C3 (the ring carbon to which C_β is attached; analog of C1 in Tyr) in a way similar to Eq. 4. Such a hypothesis, however should be undertaken with caution since the indole ring, unlike phenoxyl ring, does not have the axial symmetry associated with the x axis. So, although it is reasonable to suggest that a relationship similar to Eq. 4 would be valid for tryptophanyl radicals (the higher the ρ_{C3}, the lower the g_x), such a relationship might be not linear.

Is there any experimental data to support our structural assignments? X-ray crystallography looks at the structure of a tyrosine in a crystal, whereas EPR looks at frozen solution structures of tyrosine radicals. Adding/subtracting an electron, or going to the crystal state, might perturb the rotation angle. Although being aware of these caveats, it is nevertheless instructive to compare the angles determined by EPR with those obtained from the published protein structure to see if there are cases where we have good agreement. EPR methods alone always yield two possible values for the phenoxyl ring rotation angle (Table 1). When there is a consensus about the location of the radical in proteins (*S. typhimurium*, *E. coli*, mouse RNR, and ovine PGHS wide doublet), one of the two optimal θ-values is always in a good agreement with the value found from the crystal structure for the corresponding Tyr residues, indicating consistency in the values of the rotation angle found by the two different methods (Table 1). When the location of the radical is not known, or there is only a tentative assignment in the literature, we suggest a method of creation of a shortlist of tyrosine residues in the protein with a rotational conformation close to either of the two optimal θ-values (Svistunenko et al., 2003).

For example, the optimal θ-value for the tyrosyl radical in HH Mb ($-32°$ or $-28°$) allows us to unambiguously identify the residue as Tyr^{103} ($\theta = -31.7°$, Table 1) since the only other tyrosine (Tyr^{146}) is characterized by $\theta = -57.5°$, which is markedly different from either of the optimal θ-values. Our identification of Tyr^{103} as the site of the radical in the HH metMb/H_2O_2 system is in agreement with earlier assignment of this radical, also based on an analysis of the EPR spectral lineshape (Gunther et al., 2000). The (presumably identical) radical that can be spin-trapped in the HH Mb/H_2O_2 system by 2-methyl-2-nitrosopropane (Fenwick and English, 1996) or by 3,5-dibromo-4-nitrosobenzene sulfonate (Harris et al., 2002) was also demonstrated to be located on Tyr^{103} by the use of mass spectrometry (Fenwick and English, 1996) and by a combination of EPR, electrophoretic purification, and mass spectrometry (Harris et al., 2002).

The radical in Lg was hypothesized to be located on Tyr^{133}, the closest tyrosine to the heme (Davies and Puppo, 1992). Indeed, the value of angle θ in this residue, when averaged over two identical chains, is $52.0°$, as can be found from structure file 1BIN (Hargrove et al., 1997). This value is only $7°$ different from the angle of $45°$ obtained from our simulation (Table 1). Two other tyrosine residues in this protein, Tyr^{25} and Tyr^{30}, are less probable candidates, in that the corresponding averaged angles for these residues are $8.5°$ and $28.7°$, respectively—which are $36.5°$ and $16.3°$ different from the angle of $45°$. Thus, by the closeness of angle θ in the three tyrosine residues to the angle found from the simulation—$7°$ for Tyr^{133}, $16.3°$ for Tyr^{30}, and $36.5°$ for Tyr^{25}—the first residue, Tyr^{133}, is indeed the most likely site to host the radical (Table 1), whereas the other two tyrosine residues present in Lg are far less probable candidates.

No residue assignment has been given so far to the radical in human metHb. Our analysis of a total of 12 Tyr residues in Hb (structure file 1HGB; Liddington et al., 1992) have shown that Tyr^{42} in the α-subunits is the most probable site of the free radical location since angle $\theta = 53°$ obtained from the simulation is only $3.5°$ different from the value of this angle averaged over two homologous α-subunits ($\theta = 56.5°$). Two other sites, Tyr^{130} and Tyr^{35} in the β-subunits, should be considered as "next most probable" since the values of their angle averaged over the two homologous β-subunits are $7.8°$ and $8.8°$ different from the value of $53°$ obtained from the simulation.

In bigger proteins with a large number of Tyr residues the analysis can be more laborious. Nevertheless, a residue responsible for the radical can sometimes still be singled out. For example, the radical in *P. denitrificans* CcO was tentatively assigned to the active site Tyr^{280} (MacMillan et al., 1999). Our recent data showed, however, that the rotational conformation of Tyr^{280} is inconsistent with the

radical being on this residue (Svistunenko et al., 2003). Instead, our analysis points to Tyr[167] (Table 1) as the most probable site (of a total of 37 tyrosine residues present in *P. denitrificans* C*c*O) that could host the observed radical (Svistunenko et al., 2003). Tyr[167] is a highly conserved residue and is close to the active site. Interestingly, our algorithm shows that the homologous residue in the bovine C*c*O (Tyr[129]) can be responsible (Svistunenko et al., 2003) for the EPR spectrum observed in this enzyme and previously assigned to a tryptophan residue (Rigby et al., 2000). We find it particularly intriguing that our algorithm predicts the rotational conformation of a hypothetical tyrosyl radical in the bovine C*c*O very close to the rotational conformation of Tyr[129]—the residue, homologous to Tyr[167] in the *P. denitrificans* C*c*O, to which we have assigned the radical in this enzyme quite confidently. Clearly, more studies are required to resolve the contradiction between previous interpretations and our assignment of the radical in bovine C*c*O.

CONCLUSIONS

We propose a universal algorithm for finding all parameters necessary for the simulation of a tyrosyl radical EPR spectrum. The algorithm bluntly specifies the values for all conserved simulation parameters (the same set for all radicals) and calculates the 10 nonconserved parameters while employing only two input variables: the spin density on atom C1 and the phenoxyl ring rotation angle. Our method makes it possible for the first time to perform a global simulation of all known lineshapes when using a common algorithm.

The algorithm is largely based on our finding that the principal *g*-values of a tyrosyl radical can be presented as polynomial functions of ρ_{C1}, the dependence of g_x on ρ_{C1} being linear. This has a particular practical importance, since g_x can be measured directly by HF EPR.

Our algorithm makes it easy to determine whether an observed EPR spectrum arises from a tyrosyl radical and whether the radical has an H-bond. The recipe is simple: take an HF spectrum and measure the g_x-value; find ρ_{C1} by using Eq. 4; and use this value as the input parameter in the algorithm and vary the other parameter, angle θ, to achieve a good fit to the experimental X-band spectrum. If the HF spectrum is not available, both parameters, θ and ρ_{C1}, will have to be varied, although ρ_{C1} should only be varied within a narrow interval of 0.34–0.43. If $\rho_{C1} > 0.38$, the radical is likely to be H-bonded, and if the g_x-component in the experimental HF spectrum is markedly broader than in the simulated spectrum, the strength of the H-bond (as well as ρ_{C1}) is distributed. If a spectrum cannot be simulated using this method, it is highly unlikely that it originates from a tyrosyl radical.

A simulation based on our algorithm results in finding the values of ρ_{C1} and θ with unprecedented accuracy. Our new

online database, dedicated to ranking all Tyr residues in proteins by angle θ, significantly helps in finding the residue responsible for the radical. In many cases an unambiguous assignment of the tyrosyl radical can be performed. Where this is not the case, our method generates a shortlist of most likely ''tyrosine candidate sites,'' ready to be tested one-by-one by alternative methods—e.g., site-directed mutagenesis.

SUPPLEMENTARY MATERIAL

The following supplementary materials are available in a single archive file by visiting BJ Online at http://www.biophysj.org: the document *Algorithm Description.pdf* (Figs. S1–S10, Tables S1–S6, Eqs. S1–S19); Excel file calculators (*algorithm.xls*, *theta_in_tyr.xls*, *g_*, and *_k.xls*); and the folder *Simulation Data*.

REFERENCES

Allard, P., A. L. Barra, K. K. Andersson, P. P. Schmidt, M. Atta, and A. Gräslund. 1996. Characterization of a new tyrosyl free radical in *Salmonella typhimurium* ribonucleotide reductase with EPR at 9.45 and 245 GHz. *J. Am. Chem. Soc.* 118:895–896.

Babcock, G. T., M. K. El-Deeb, P. O. Sandusky, M. M. Whittaker, and J. W. Whittaker. 1992. Electron-paramagnetic resonance and electron nuclear double-resonance spectroscopies of the radical site in galactose-oxidase and of thioether-substituted phenol model compounds. *J. Am. Chem. Soc.* 114:3727–3734.

Bender, C. J., M. Sahlin, G. T. Babcock, B. A. Barry, T. K. Chandrashekar, S. P. Salowe, J. Stubbe, B. Lindström, L. Petersson, A. Ehrenberg, and B.-M. Sjöberg. 1989. An ENDOR study of the tyrosyl free radical in ribonucleotide reductase from *Escherichia coli*. *J. Am. Chem. Soc.* 111:8076–8083.

Chouchane, S., S. Girotto, S. Yu, and R. S. Magliozzo. 2002. Identification and characterization of tyrosyl radical formation in *Mycobacterium tuberculosis* catalase-peroxidase (KatG). *J. Biol. Chem.* 277:42633–42638.

Davies, M. J., and A. Puppo. 1992. Direct detection of a globin-derived radical in leghemoglobin treated with peroxides. *Biochem. J.* 281:197–201.

DeGray, J. A., G. Lassmann, J. F. Curtis, T. A. Kennedy, L. J. Marnett, T. E. Eling, and R. P. Mason. 1992. Spectral analysis of the protein-derived tyrosyl radicals from prostaglandin H synthase. *J. Biol. Chem.* 267:23583–23588.

Di Bilio, A. J., B. R. Crane, W. A. Wehbi, C. N. Kiser, M. M. Abu-Omar, R. M. Carlos, J. H. Richards, J. R. Winkler, and H. B. Gray. 2001. Properties of photogenerated tryptophan and tyrosyl radicals in structurally characterized proteins containing rhenium(I) tricarbonyl diimines. *J. Am. Chem. Soc.* 123:3181–3182.

Dorlet, P., A. W. Rutherford, and S. Un. 2000. Orientation of the tyrosyl D, pheophytin anion, and semiquinone Q_A^- radicals in photosystem II determined by high-field electron paramagnetic resonance. *Biochemistry.* 39:7826–7834.

Dorlet, P., S. A. Seibold, G. T. Babcock, G. J. Gerfen, W. L. Smith, A. L. Tsai, and S. Un. 2002. High-field EPR study of tyrosyl radicals in prostaglandin H_2 synthase-1. *Biochemistry.* 41:6107–6114.

Eriksson, M., A. Jordan, and H. Eklund. 1998. Structure of *Salmonella typhimurium* nrdF ribonucleotide reductase in its oxidized and reduced forms. *Biochemistry.* 37:13359–13369.

Farrar, C. T., G. J. Gerfen, R. G. Griffin, D. A. Force, and R. D. Britt. 1997. Electronic structure of the Y_D tyrosyl radical in photosystem II: a high-frequency electron paramagnetic resonance spectroscopic and density functional theoretical study. *J. Phys. Chem. B.* 101:6634–6641.

Fenwick, C. W., and A. M. English. 1996. Trapping and LC-MS identification of protein radicals formed in the horse heart metmyoglobin-H_2O_2 reaction. *J. Am. Chem. Soc.* 118:12236–12237.

Fessenden, R. W., and R. H. Schuler. 1963. Electron spin resonance studies of transient alkyl radicals. *J. Chem. Phys.* 39:2147–2195.

Frey, P. A. 2001. Radical mechanisms of enzymatic catalysis. *Annu. Rev. Biochem.* 70:121–148.

Gerfen, G. J., B. F. Bellew, S. Un, J. M. Bollinger, J.-A. Stubbe, R. G. Griffin, and D. J. Singel. 1993. High-frequency (139.5 GHz) EPR spectroscopy of the tyrosyl radical in *Escherichia coli* ribonucleotide reductase. *J. Am. Chem. Soc.* 115:6420–6421.

Gunther, M. R., B. E. Sturgeon, and R. P. Mason. 2000. A long-lived tyrosyl radical from the reaction between horse metmyoglobin and hydrogen peroxide. *Free Radic. Biol. Med.* 28:709–719.

Gunther, M. R., R. A. Tschirret-Guth, H. E. Witkowska, Y. C. Fann, D. P. Barr, P. R. Ortiz de Montellano, and R. P. Mason. 1998. Site-specific spin trapping of tyrosine radicals in the oxidation of metmyoglobin by hydrogen peroxide. *Biochem. J.* 330:1293–1299.

Hargrove, M. S., J. K. Barry, E. A. Brucker, M. B. Berry, G. N. Phillips, Jr., J. S. Olson, R. Arredondo-Peter, J. M. Dean, R. V. Klucas, and G. Sarath. 1997. Characterization of recombinant soybean leghemoglobin *a* and apolar distal histidine mutants. *J. Mol. Biol.* 266:1032–1042.

Harrenga, A., and H. Michel. 1999. The cytochrome *c* oxidase from *Paracoccus denitrificans* does not change the metal center ligation upon reduction. *J. Biol. Chem.* 274:33296–33299.

Harris, M. N., S. W. Burchiel, P. G. Winyard, J. R. Engen, C. D. Mobarak, and G. S. Timmins. 2002. Determining the site of spin trapping of the equine myoglobin radical by combined use of EPR, electrophoretic purification, and mass spectrometry. *Chem. Res. Toxicol.* 15:1589–1594.

Himo, F., A. Gräslund, and L. A. Eriksson. 1997. Density functional calculations on model tyrosyl radicals. *Biophys. J.* 72:1556–1567.

Hofbauer, W., A. Zouni, R. Bittl, J. Kern, P. Orth, F. Lendzian, P. Fromme, H. T. Witt, and W. Lubitz. 2001. Photosystem II single crystals studied by EPR spectroscopy at 94 GHz: the tyrosine radical Y_D?. *Proc. Natl. Acad. Sci. USA.* 98:6623–6628.

Hoganson, C. W., and G. T. Babcock. 1992. Protein-tyrosyl radical interactions in photosystem II studied by electron spin resonance and electron nuclear double resonance spectroscopy: comparison with ribonucleotide reductase and *in vitro* tyrosine. *Biochemistry.* 31:11874–11880.

Hoganson, C. W., M. Sahlin, B.-M. Sjöberg, and G. T. Babcock. 1996. Electron magnetic resonance of the tyrosyl radical in ribonucleotide reductase from *Escherichia coli*. *J. Am. Chem. Soc.* 118:4672–4679.

Hsi, L. C., C. W. Hoganson, G. T. Babcock, and W. L. Smith. 1994. Characterization of a tyrosyl radical in prostaglandin endoperoxide synthase-2. *Biochem. Biophys. Res. Commun.* 202:1592–1598.

Ivancich, A., P. Dorlet, D. B. Goodin, and S. Un. 2001a. Multifrequency high-field EPR study of the tryptophanyl and tyrosyl radical intermediates in wild-type and the W191G mutant of cytochrome *c* peroxidase. *J. Am. Chem. Soc.* 123:5050–5058.

Ivancich, A., G. Mazza, and A. Desbois. 2001b. Comparative electron paramagnetic resonance study of radical intermediates in turnip peroxidase isozymes. *Biochemistry.* 40:6860–6866.

Ivancich, A., H. M. Jouve, and J. Gaillard. 1996. EPR evidence for a tyrosyl radical intermediate in bovine liver catalase. *J. Am. Chem. Soc.* 118:12852–12853.

Ivancich, A., T. A. Mattioli, and S. Un. 1999. Effect of protein microenvironment on tyrosyl radicals. A high-field (285 GHz) EPR, resonance Raman, and hybrid density functional study. *J. Am. Chem. Soc.* 121:5743–5753.

Kauppi, B., B. B. Nielsen, S. Ramaswamy, I. K. Larsen, M. Thelander, L. Thelander, and H. Eklund. 1996. The three-dimensional structure of mammalian ribonucleotide reductase protein R2 reveals a more-accessible iron-radical site than *Escherichia coli* R2. *J. Mol. Biol.* 262:706–720.

Ko, T. P., J. Day, A. J. Malkin, and A. McPherson. 1999. Structure of orthorhombic crystals of beef liver catalase. *Acta Crystallogr. D Biol. Crystallogr.* 55:1383–1394.

Kulmacz, R. J., Y. Ren, A. L. Tsai, and G. Palmer. 1990. Prostaglandin H synthase: spectroscopic studies of the interaction with hydroperoxides and with indomethacin. *Biochemistry.* 29:8760–8771.

Liddington, R., Z. Derewenda, E. Dodson, R. Hubbard, and G. Dodson. 1992. High resolution crystal structures and comparisons of T-state deoxyhaemoglobin and two liganded T-state haemoglobins: T(α-oxy)-haemoglobin and T(met)haemoglobin. *J. Mol. Biol.* 228:551–579.

Loll, P. J., D. Picot, O. Ekabo, and R. M. Garavito. 1996. Synthesis and use of iodinated nonsteroidal antiinflammatory drug analogs as crystallo-graphic probes of the prostaglandin H2 synthase cyclooxygenase active site. *Biochemistry.* 35:7330–7340.

MacMillan, F., A. Kannt, J. Behr, T. Prisner, and H. Michel. 1999. Direct evidence for a tyrosine radical in the reaction of cytochrome *c* oxidase with hydrogen peroxide. *Biochemistry.* 38:9179–9184.

Maurus, R., C. M. Overall, R. Bogumil, Y. Luo, A. G. Mauk, M. Smith, and G. D. Brayer. 1997. A myoglobin variant with a polar substitution in a conserved hydrophobic cluster in the heme binding pocket. *Biochim. Biophys. Acta.* 1341:1–13.

McConnell, H. M., and D. B. Cheshunt. 1958. Theory of isotropic hyperfine interaction in π-electron radicals. *J. Chem. Phys.* 28:107–117.

Miki, H., K. Harada, I. Yamazaki, M. Tamura, and H. Watanabe. 1989. Electron-spin resonance spectrum of Tyr[151] free radicals formed in reactions of sperm whale metmyoglobin with ethyl hydroperoxide and potassium irridate. *Arch. Biochem. Biophys.* 275:354–362.

Nordlund, P., and H. Eklund. 1993. Structure and function of the *Escherichia coli* ribonucleotide reductase protein R2. *J. Mol. Biol.* 232:123–164.

Reeder, B. J., M. A. Sharpe, A. D. Kay, M. Kerr, K. Moore, and M. T. Wilson. 2002. Toxicity of myoglobin and haemoglobin: oxidative stress in patients with rhabdomyolysis and subarachnoid haemorrhage. *Biochem. Soc. Trans.* 30:745–748.

Reichard, P., and A. Ehrenberg. 1983. Ribonucleotide reductase—a radical enzyme. *Science.* 221:514–519.

Rigby, S. E., S. Junemann, P. R. Rich, and P. Heathcote. 2000. Reaction of bovine cytochrome *c* oxidase with hydrogen peroxide produces a tryptophan cation radical and a porphyrin cation radical. *Biochemistry.* 39:5921–5928.

Rigby, S. E., J. H. Nugent, and P. J. O'Malley. 1994. The dark stable tyrosine radical of photosystem II studied in three species using ENDOR and EPR spectroscopies. *Biochemistry.* 33:1734–1742.

Sahlin, M., A. Gräslund, A. Ehrenberg, and B.-M. Sjöberg. 1982. Structure of the tyrosyl radical in bacteriophage T4-induced ribonucleotide reductase. *J. Biol. Chem.* 257:366–369.

Sahlin, M., L. Petersson, A. Gräslund, A. Ehrenberg, B. M. Sjöberg, and L. Thelander. 1987. Magnetic interaction between the tyrosyl free radical and the antiferromagnetically coupled iron center in ribonucleotide reductase. *Biochemistry.* 26:5541–5548.

Schmidt, P. P., K. K. Andersson, A.-L. Barra, L. Thelander, and A. Gräslund. 1996. High-field EPR studies of mouse ribonucleotide reductase indicate hydrogen-bonding of the tyrosyl radical. *J. Biol. Chem.* 271:23615–23618.

Selinsky, B. S., K. Gupta, C. T. Sharkey, and P. J. Loll. 2001. Structural analysis of NSAID binding by prostaglandin H2 synthase: time-dependent and time-independent inhibitors elicit identical enzyme conformations. *Biochemistry.* 40:5172–5180.

Shi, W., C. W. Hoganson, M. Espe, C. J. Bender, G. T. Babcock, G. Palmer, R. J. Kulmacz, and A. Tsai. 2000. Electron paramagnetic resonance and electron nuclear double resonance spectroscopic identi-fication and characterization of the tyrosyl radicals in prostaglandin H synthase 1. *Biochemistry.* 39:4112–4121.

Svistunenko, D. A., J. Dunne, M. Fryer, P. Nicholls, B. J. Reeder, M. T. Wilson, M. G. Bigotti, F. Cutruzzola, and C. E. Cooper. 2002. Comparative study of tyrosine radicals in hemoglobin and myoglobins treated with hydrogen peroxide. *Biophys. J.* 83:2845–2855.

Svistunenko, D. A., M. A. Sharpe, P. Nicholls, C. Blenkinsop, N. A. Davies, J. Dunne, M. T. Wilson, and C. E. Cooper. 2000. The pH dependence of naturally occurring low-spin forms of methaemoglobin and metmyoglobin: an EPR study. *Biochem. J.* 351:595–605.

Svistunenko, D. A., M. T. Wilson, and C. E. Cooper. 2003. Tryptophan or tyrosine? On the nature of the amino acid radical formed following hydrogen peroxide treatment of cytochrome *c* oxidase. *Biochim. Biophys. Acta*. n press.

Tommos, C., X.-S. Tang, K. Warncke, C. W. Hoganson, S. Styring, J. McCracken, B. A. Diner, and G. T. Babcock. 1995. Spin-density distribution, conformation, and hydrogen bonding of the redox-active tyrosine Y_z in photosystem II from multiple-electron magnetic-resonance spectroscopies: implications for photosynthetic oxygen evolution. *J. Am. Chem. Soc.* 117:10325–10335.

Warncke, K., G. T. Babcock, and J. McCracken. 1994. Structure of the Y_D tyrosine radical in photosystem II as revealed by ^{2}H electron spin echo envelope modulation (ESEEM) spectroscopic analysis of hydrogen hyperfine interactions. *J. Am. Chem. Soc.* 116:7332–7340.

Warncke, K., and M. S. Perry. 2001. Redox state dependence of rotamer distributions in tyrosine and neutral tyrosyl radicals. *Biochim. Biophys. Acta*. 1545:1–5.

Whittaker, M. M., W. R. Duncan, and J. W. Whittaker. 1996a. Synthesis, structure, and properties of a model for galactose oxidase. *Inorg. Chem.* 35:382–386.

Whittaker, M. M., P. J. Kersten, N. Nakamura, J. Sandersloehr, E. S. Schweizer, and J. W. Whittaker. 1996b. Glyoxal oxidase from *Phanerochaete chrysosporium* is a new radical-copper oxidase. *J. Biol. Chem.* 271:681–687.